Journal of
Applied Crystallography
ISSN 0021-8898

Received 27 February 2004
Accepted 10 September 2004

Size–strain line-broadening analysis of the ceria round-robin sample

D. Balzar,[a,b]* N. Audebrand,[c] M. R. Daymond,[d] A. Fitch,[e] A. Hewat,[f] J. I. Langford,[g] A. Le Bail,[h] D. Louër,[c] O. Masson,[e] C. N. McCowan,[b] N. C. Popa,[i] P. W. Stephens[j] and B. H. Toby[k]

[a]Department of Physics and Astronomy, University of Denver, 2112 E. Wesley Ave., Denver, CO 80208, USA, [b]National Institute of Standards and Technology, Boulder, CO 80305, USA, [c]Laboratoire de Chimie du Solide et Inorganique Moléculaire (CNRS UMR 6511), Institut de Chimie, Université de Rennes, Avenue du Général Leclerc, 35042 Rennes Cedex, France, [d]ISIS Facility, Rutherford-Appleton Laboratories, Didcot, OX11 0QX, UK, [e]ESRF, BP 220, F-38043 Grenoble Cedex, France, [f]ILL, F-38043 Grenoble Cedex, France, [g]University of Birmingham, Birmingham, UK, [h]Université du Maine, Laboratoire des Fluorures, CNRS UMR 6010, Avenue O. Messiaen, 72085 Le Mans Cedex 9, France, [i]National Institute for Materials Physics, PO Box MG-7, Bucharest, Romania, [j]Department of Physics and Astronomy, State University of New York, Stony Brook, NY 11794-3800, USA, and [k]NCNR, National Institute of Standards and Technology, Gaithersburg, Maryland, USA. Correspondence e-mail: balzar@du.edu

The results of both a line-broadening study on a ceria sample and a size–strain round robin on diffraction line-broadening methods, which was sponsored by the Commission on Powder Diffraction of the International Union of Crystallography, are presented. The sample was prepared by heating hydrated ceria at 923 K for 45 h. Another ceria sample was prepared to correct for the effects of instrumental broadening by annealing commercially obtained ceria at 1573 K for 3 h and slowly cooling it in the furnace. The diffraction measurements were carried out with two laboratory and two synchrotron X-ray sources, two constant-wavelength neutron and a time-of-flight (TOF) neutron source. Diffraction measurements were analyzed by three methods: the model assuming a lognormal size distribution of spherical crystallites, Warren–Averbach analysis and Rietveld refinement. The last two methods detected a relatively small strain in the sample, as opposed to the first method. Assuming a strain-free sample, the results from all three methods agree well. The average real crystallite size, on the assumption of a spherical crystallite shape, is 191 (5) Å. The scatter of results given by different instruments is relatively small, although significantly larger than the estimated standard uncertainties. The Rietveld refinement results for this ceria sample indicate that the diffraction peaks can be successfully approximated with a pseudo-Voigt function. In a common approximation used in Rietveld refinement programs, this implies that the size-broadened profile cannot be approximated by a Lorentzian but by a full Voigt or pseudo-Voigt function. In the second part of this paper, the results of the round robin on the size–strain line-broadening analysis methods are presented, which was conducted through the participation of 18 groups from 12 countries. Participants have reported results obtained by analyzing data that were collected on the two ceria samples at seven instruments. The analysis of results received in terms of coherently diffracting, both volume-weighted and area-weighted apparent domain size are reported. Although there is a reasonable agreement, the reported results on the volume-weighted domain size show significantly higher scatter than those on the area-weighted domain size. This is most likely due to a significant number of results reporting a high value of strain. Most of those results were obtained by Rietveld refinement in which the Gaussian size parameter was not refined, thus erroneously assigning size-related broadening to other effects. A comparison of results with the average of the three-way comparative analysis from the first part shows a good agreement.

© 2004 International Union of Crystallography
Printed in Great Britain – all rights reserved

1. Introduction

The broadening of diffraction lines occurs for two principal reasons: instrumental effects and physical origins [for the most current review articles on this subject, consult the recent monographs edited by Snyder *et al.* (1999) and Mittemeijer & Scardi (2004)]. The latter can be roughly divided into diffraction-order-independent (size) and diffraction-order-dependent (strain) broadening in reciprocal space. Because many common crystalline defects cause line broadening to behave in a similar way, it is often difficult to discern the type of defect dominating in a particular sample. Therefore, it would be desirable to have standard samples with different types of defects to help to characterize unequivocally the particular sample under the investigation.

Another point for consideration is the analysis of line broadening for the purpose of extracting information about crystallite size and structure imperfections. Quantification of line-broadening effects is not trivial and there are different and sometimes conflicting methods. Roughly, they can be divided into two types: phenomenological 'top–bottom' approaches, such as integral-breadth methods (summarized by Klug & Alexander, 1974; see also Langford, 1992) and Fourier methods (Bertaut, 1949; Warren & Averbach, 1952). Both approaches estimate physical quantities (coherently diffracting domain size and lattice distortion/strain averaged over a particular distance in the direction of the diffraction vector) from diffraction line broadening. Only after the analysis, is an attempt made to connect the thus-obtained parameters with actual (i) defects and strains in the sample, based on the behavior of certain parameters and a rather loose association with underlying physical effects (see, for instance, Warren, 1959), or (ii) crystallite size and shape in strain-free samples (see, for example, Louër *et al.*, 1983). Conversely, there are physically based 'bottom–top' approaches that attempt to model the influence of simplified dislocation configurations (Krivoglaz, 1996; Ungár, 1999) or similar defects (van Berkum, 1994), or crystallite size distributions (Langford *et al.*, 2000) on diffraction lines. Conditionally, we can call these two approaches *a posteriori* and *a priori*, respectively, according to when the correspondence of domain size and strain parameters with the underlying microstructure is made. Lately, there have been significant efforts (Ungár *et al.*, 2001, and references therein) to bridge these sometimes diverging approaches. Even among the *a posteriori* approaches, there are a variety of methods that yield conflicting results for identically defined physical quantities. Simplified integral-breadth methods that assume either a Gaussian or Lorentzian function for a size- and/or strain-broadened profile were shown to yield systematically different results (Balzar & Popović, 1996). Nowadays, it is widely accepted that a 'double-Voigt' approach, that is, a Voigt-function approximation for both size-broadened and strain-broadened profiles (Langford, 1980, 1992; Balzar, 1992) is a better model than the simplified integral-breadth methods. This model also agrees with the Warren–Averbach (1952) analysis on the assumption of a Gaussian distribution of strains (Balzar & Ledbetter, 1993; Balzar, 1999). However, it fails in cases when observed profiles cannot be approximated by a Voigt function or when an assumed size-broadened Voigt profile yields negative column-length size distribution [the significance of the latter in different contexts, consequences, and possible corrections were discussed by Young *et al.* (1967), Warren (1969), Balzar & Ledbetter (1993), and Popa & Balzar (2002)]. Despite the attempts to assess systematic differences between results obtained by different line-broadening methods, generally any comparison is difficult because of the different definition of parameters and procedures. Hence, a rational way to assess the reliability of results yielded by different methods is an empiric approach, such as by means of a round robin.

To perform successfully such a broad effort as the round robin, we decided upon a sample with a simple crystal structure with well defined physical and chemical properties; therefore, a specimen was selected with a relatively narrow crystallite size distribution of predominantly spherical shape, on average, thus yielding line broadening that is independent of crystallographic direction (isotropic). To reduce the propagation of errors associated with the instability of the deconvolution operation, the conditions for sample preparation were monitored to produce an optimal diffraction line broadening. Furthermore, because the separation of size and strain effects is a separate and complicated problem, the intent was to obtain a negligible or small amount of strain in the sample. Line-broadening analysis strongly depends on the correction for instrumental effects and the details of peak shape, particularly line profile tails. For that reason, measurements were collected with different radiations and with different resolutions and experimental setups. To our knowledge, this is the first attempt to collect the measurements on the same sample with such a different array of instruments.

This paper has two parts. The aim of the first part is to give an account of the specimen preparation and to characterize the measurements undertaken at different instruments. This is required in order to ensure the self-consistency of measurements before round-robin data are made available to the round-robin participants. The participants then can use different methods to analyze the measurements. Here, we give the results of analyses by three methods: Bayesian deconvolution followed by the Warren–Averbach (1952) analysis of line broadening, as a least-biased phenomenological approach, an assumed physical model of lognormal size distribution of spherical crystallites, and Rietveld (1969) refinement, in order to assess potential correlations with other parameters and subsequent possible systematic errors in size–strain parameters. The application of Rietveld refinement is especially important, as this route is becoming increasingly used for the determination not only of structural but also microstructural information about the sample, but often without a clear understanding of the connection between refined profile parameters and the physical parameters of interest. For this reason, we discuss it in more detail in §3.3. By using three different line-broadening analysis methods on all the measurements in a consistent manner, we can better assess

the accuracy of the size–strain results, as well as both the advantages and drawbacks of different analysis routes. The aim of the second part (§5) is to present the results of the round robin where the participants used different methods of line-broadening analysis to evaluate size and strain. We begin with the details about the round robin and go over basic definitions of the quantities (§5.1), and compare and discuss the results (§5.2).

2. Experimental

2.1. Preparation of ceria powders

2.1.1. Round-robin sample. Nanocrystalline CeO_2 was prepared by thermal treatment of hydrated ceria, according to the method reported in detail elsewhere (Audebrand *et al.*, 2000). Hydrated ceria was precipitated at room temperature from the addition of $Ce(SO_4)_2.4H_2O$ (Merck[1]) to a 1 *M* ammonia solution. The obtained precursor consists of ultrafine yellow hydrated cerium oxide $CeO_2.xH_2O$ with spherical crystallites of about 20 Å diameter, on average. It has been reported that the thermal treatment of this precursor in the temperature range 873–1173 K leads to the formation of a CeO_2 sample with average spherical crystallites characterized by a volume-weighted diameter in the range 263–1756 Å (Audebrand *et al.*, 2000). In order to obtain a sample that would not produce too much diffraction line broadening, the annealing temperature was selected to be 923 K. The hydrated ceria was heated in a silica crucible at 120 K h^{-1} to 923 K, and then kept for 45 h at this temperature in order to ensure complete annealing. From this procedure, 50 g of CeO_2 was obtained (here designated as S1). The microstructural homogeneity of the entire powder was checked by collecting X-ray diffraction data for samples located at the bottom and the top of the crucible.

2.1.2. Instrumental-standard sample. If we denote the instrumental, physical and observed profiles by $g(x)$, $p(x)$ and $h(x)$, respectively, the observed Bragg profile is

$$h(x) = \int p(z)g(x - z)\,\mathrm{d}z + b(x) + n(x), \qquad (1)$$

where $b(x)$ is the background and $n(x)$ the noise [$\langle n(x)\rangle = 0$].

In the determination of g, there are several possible ways to correct for broadening effects due to the various instruments. Lately, much work has been carried out on modeling different contributions to diffraction line shape by laboratory instruments (Wilson, 1963; Klug & Alexander, 1974; Cheary & Coelho, 1992). However, because of the very different instruments discussed here, we preferred to characterize instrumental broadening by measuring a suitable sample that shows a minimal amount of physical line broadening caused by defects and small crystallite size. The National Institute of Standards and Technology (NIST) makes available the Standard Reference Material SRM660a LaB_6 for this purpose. However, this material is not suitable as a standard in this case for several reasons: (i) LaB_6 cannot be used with neutrons because of boron; (ii) there is a difference in the linear absorption coefficients by approximately a factor of 2 between LaB_6 and CeO_2, which would introduce an additional transparency broadening and, consequently, systematic errors in the results; (iii) Bragg reflections at different diffracting angles for the standard and the sample under investigation are a potential source of systematic errors in line-broadening analysis, especially for deconvolution methods [see, for instance, a review by Delhez *et al.* (1980) for correcting systematic errors for improper standards]. Thus, we opted for annealed ceria. Commercially obtained (Nanotech[1]) ceria was annealed at different temperatures and times to achieve minimal line broadening while not inducing too much grain growth, which would be detrimental to the counting statistics and shape of the diffraction line profiles. This is a potential issue in particular with synchrotron measurements. An optimum behavior was obtained by annealing at 1573 K for 3 h in air. The powder was slowly cooled overnight in the crucible. This sample is designated here as S2. Fig. 1 shows the full width at half-maximum (FWHM) for all available Bragg reflections for the samples S1, S2 and NIST new SRM660a LaB_6, as determined from precise measurements using a high-resolution Bragg–Brentano diffractometer with monochromatic X-rays (Cu $K\alpha_1$ radiation). The instrument characteristics have been reported previously (Louër & Langford, 1988). The comparison between annealed CeO_2 and a NIST SRM660a LaB_6 powder, when used for correction of instrumental broadening, did not show significant changes (within a single standard deviation) in the final parameters of interest, namely domain size and strain values.

2.2. Measurements

2.2.1. Morphology. We used field-emission scanning electron microscopy (FESEM) to characterize the ceria powder (S1). Micrographs have shown the prevailing shape of the particles to be spherical and the grain size distribution could

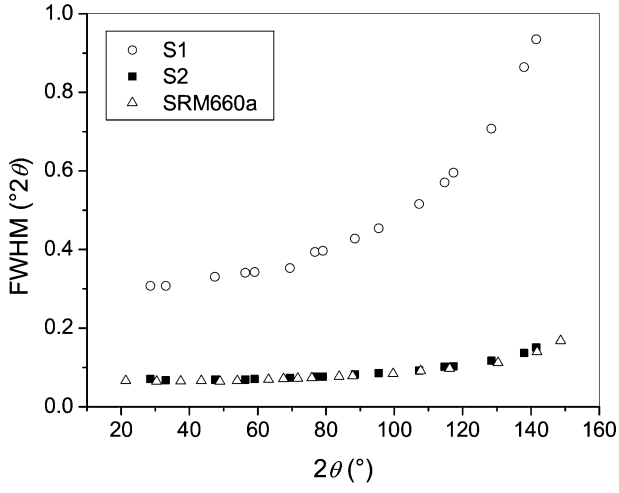

Figure 1
FWHM *versus* diffraction angle, as obtained from laboratory X-ray measurements, for three samples: CeO_2 with broadened lines (sample S1), annealed CeO_2 used to correct for instrumental effects (sample S2), and new NIST SRM660a LaB_6.

[1] Commercial names are given for identification purposes only.

Table 1
Data collection conditions at different instruments.

Instrument	Wavelength (Å)	Geometry	Optics	Detector	Data collection parameters in 2θ (θ is the diffraction angle)
High-resolution laboratory X-ray (Birmingham)	Cu $K\alpha_1$	Flat-plate Bragg–Brentano	Incident beam: Ge (111) flat monochromator, 1.4° equatorial and 1.8° axial divergence; diffracted beam: 2° Soller slits, 0.05° receiving slit	Scintillation	Three ranges: (i) 20.0–64.5°, 0.01° step, 20 s step^{-1}; (ii) 64.5–102.5°, 0.02° step, 70 s step^{-1}; (iii) 102.5–150.0°, 0.02° step, 80 s step^{-1}
Commercial laboratory X-ray (Le Mans)	Cu $K\alpha_{1,2}$ doublet	Flat-plate Bragg–Brentano	Incident beam: 2° Soller slits, variable slits (the intensity corrected for the factor $1/\sin\theta$ was used for the analysis); diffracted beam: graphite monochromator, 0.1 mm receiving slit	Proportional	20–150°, 0.01° step, 46 s step^{-1} (sample S2), and 60 s step^{-1} (sample S1)
Third-generation synchrotron (ESRF BM16)	0.39982	Capillary Debye–Scherrer	Incident beam: double-crystal Si (111) flat monochromator; diffracted beam: nine Ge (333) flat analyzer crystals covering 16° in 2θ	Nine scintillation	3–29.2°, 0.0004° step, 1.2 s step^{-1} (sample S2), and 0.004° step, 12 s step^{-1} (sample S1)
Second-generation synchrotron (NSLS X3B1)	0.6998	Flat-plate parallel beam	Incident beam: double (111) Si monochromator; diffracted beam: Ge (111) flat analyzer crystal	Scintillation	12–60°, 0.002° step (sample S2), and 2–79.22°, 0.01° step (sample S1)
CW neutron (ILL D1A)	1.91	Container Debye–Scherrer	Incident beam: focusing Ge (111) monochromator	25 detectors, 6° apart	0.05° step
CW neutron (NCNR BT-1)	1.5905	Container Debye–Scherrer	Incident beam: Si (531) monochromator at take-off angle of 120° with 7 arcmin collimation	32 detectors in 5° intervals	3–168°, 0.05° step
TOF neutron (ISIS HRPD)		Container Debye–Scherrer			160–176°

be successfully fitted by the lognormal function. However, it was very difficult to discern individual particles from the micrographs. A recent study of ceria powder reported a lognormal size distribution of crystallites (Langford *et al.*, 2000). Furthermore, Armstrong *et al.* (2004) have recently reported TEM measurements on the same ceria sample S1. Although even the TEM crystallite size distribution was unreliable for crystallite size smaller than 150 Å because of particle agglomeration, above this size it agreed well with an assumed *a priori* lognormal distribution.

2.2.2. Diffraction measurements. Both samples S1 and S2 were distributed to instrument scientists for the measurements. Raw data are available online (http://www.boulder.nist.gov/div853/balzar, http://www.du.edu/~balzar, and the CCP14 mirror http://www.ccp14.ac.uk/) and have also been deposited with the IUCr.[2] The measurements were collected with the following instruments.

(i) University of Birmingham: a high-resolution X-ray laboratory setup.

(ii) University of Maine, Le Mans: a 'common' X-ray laboratory setup.

(iii) European Synchrotron Radiation Facility (ESRF), BM16 beamline: third-generation synchrotron, capillary geometry.

(iv) National Synchrotron Light Source (NSLS), Brookhaven National Laboratory, X3B1 beamline: second-generation synchrotron, flat-plate geometry.

(v) Institute Laue-Langevin (ILL): D1A diffractometer, constant-wavelength (CW) neutron source.

(vi) National Institute of Standards and Technology (NIST) Center for Neutron Research (NCNR): BT1 diffractometer, CW neutron source.

(vii) ISIS at the Rutherford-Appleton Laboratory: High Resolution Powder Diffractometer (HRPD) on the S8 beamline, time-of-flight neutron source.

The experimental conditions for all the instruments are listed in Table 1.

3. Methodology and results

3.1. Lognormal distribution of spherical crystallites

Based on the crystallite size distribution determined by TEM (Armstrong *et al.*, 2004), we assumed a physical model of lognormal size distribution of spherical crystallites (LNSDSC) as a physically sound model to account for line broadening. This model has recently been discussed and used successfully in a number of publications (Krill & Birringer, 1998; Langford *et al.*, 2000; Scardi & Leoni, 2001; Popa & Balzar, 2002). The lognormal size distribution function can be represented as (Popa & Balzar, 2002):

$$f(R) = R^{-1}[2\pi \ln(1+c)]^{-1/2} \times \exp\{-\ln^2[R\bar{R}^{-1}(1+c)^{1/2}]/[2\ln(1+c)]\}. \quad (2)$$

Here, $\bar{R}$ is the average radius of the particles and the dimensionless ratio c is defined as

[2] Supplementary data are available from the IUCr electronic archives (Reference: KS0213). Services for accessing these data are described at the back of the journal.

$$c = \sigma_R^2/\bar{R}^2, \tag{3}$$

where σ_R^2 is the distribution dispersion.

To extract size-broadened profiles from diffraction patterns, a correction for instrumental broadening has to be performed first. For more details, see the recent reviews by Čerňanský (1999) and Reefman (1999). A Fourier deconvolution method (Stokes, 1948) is an often-used unbiased approach that yields pure physically broadened line profile. The Stokes deconvolution method is, however, prone to serious systematic errors in cases when the background level is difficult to determine due to overlapping of neighboring reflections or weak physical broadening (Delhez *et al.*, 1980). We instead used a Bayesian deconvolution following the Richardson algorithm[3] (Richardson, 1972; Kennett *et al.*, 1978). In the Richardson algorithm, the physical profile p from equation (1) is obtained by iterating the following formula:

$$p_i^{(n+1)} = p_i^{(n)} \sum_k \left[g_{ki} h'_k \Big/ \sum_j g_{kj} p_j^{(n)} \right]. \tag{4}$$

In equation (4), n is the iteration number and h'_k is the measured profile after the background subtraction. The interval in which the deconvolution is performed can contain either a single peak or a cluster of overlapping peaks. For the former, the corresponding peak from the diffraction pattern of the annealed sample is taken as the resolution function $g(x)$, after background subtraction, normalization to unit area, and reversal around the peak position is performed [note that if $p(z)$ equals a delta function then $g(x) = h(-x)$]. For the latter, one has to use an *a priori* analytical description of the resolution function and fit all the peaks of the annealed sample in this interval. To avoid this complicated step, which can introduce bias in the parameters $\bar{R}$ and c, we excluded overlapping peaks (such as 111 and 200) from the procedure and included only the peaks with negligibly small overlap: 220, 400, 422, 333/511, 440 and 620. The last two peaks were not available for the ILL measurements and 333/511 is of a low intensity for neutrons; thus, three peaks were used in the analysis of the ILL data and five for the NIST data. The linear background was determined by means of the least-squares refinement separately for each peak and subtracted prior to the deconvolution. To avoid the noise amplification during deconvolution, the iterative process must converge after a small number of steps. To fulfill this condition, the starting profile must be as close as possible to the anticipated solution. Because for most of the measurements the instrumental profile, given by the sample S2, was significantly narrower than the profile from the sample S1, we used $p_i^{(0)} = h'_i$ as a starting guess. Thus, the number of iterations was between 5, for synchrotron measurements, and 10 to 12 for NIST and ILL measurements (see also the discussion in §4). Besides the small amplification of the noise, the off-diagonal elements of the correlation matrix of $p_i^{(n)}$ are expected to be small. The profile obtained by deconvolution can then be fitted with the physical profile through the least-squares refinement assuming independent points and Poisson statistics. For the dispersions of points in the least squares, we used the following approximation: $\sigma^2[p_i^{(n)}] \simeq p_i^{(n)} + b_i$. Note that this equation is exact for $n = 0$.

[3] In a recent review of the deconvolution methods, Čerňanský (1999) gives supplementary arguments that the Richardson algorithm indeed belongs to the class of Bayesian deconvolution methods.

Table 2
Results of the fit to Bayesian-deconvoluted profiles by a model assuming a lognormal size distribution of spherical crystallites.

The first moment of the distribution $\bar{R}$, the ratio of the distribution dispersion to the square of the first moment $c = \sigma_R^2/\bar{R}^2$, and the corresponding area-weighted D_A and volume-weighted D_V domain sizes.

	$\bar{R}$ (Å)	c	D_A (Å)	D_V (Å)
Birmingham	89.0 (10)	0.187 (5)	167 (3)	223 (5)
Le Mans	90.9 (3)	0.188 (2)	171 (1)	229 (2)
ESRF	90.0 (10)	0.192 (6)	171 (4)	229 (6)
NSLS	93.3 (7)	0.177 (3)	172 (2)	228 (4)
ILL	93.0 (20)	0.173 (7)	171 (6)	225 (9)
NIST	93.0 (40)	0.184 (15)	174 (12)	232 (19)
ISIS	91.0 (10)	0.191 (4)	172 (3)	231 (5)

The profile obtained from deconvolution, $p_i^{(n)}$, with the dispersions, $\sigma^2[p_i^{(n)}]$, was fitted by the convolution of the size profile [equations (15*a*), (21), (22) of Popa & Balzar, 2002] with the strain profile, in the corresponding variables for constant wavelength or time of flight data. Although the ceria powder S1 is expected to show small (or negligible) strain broadening (Audebrand *et al.*, 2000), we allowed for this strain correction by a single Gaussian function. The peak position and area, the size distribution parameters $\bar{R}$ and c, and the Gaussian strain parameter were refined in the least-squares refinement for every profile. The strain parameter was fixed to zero in the final refinement cycles, as we did not see any improvement in the fit. Table 2 gives results that were averaged over all reflections for a particular instrument. From the distribution parameters $\bar{R}$ and c, average apparent domain sizes follow, for comparison with other methods (Popa & Balzar, 2002):

$$D_V = 3\bar{R}(1+c)^3/2 \tag{5a}$$

and

$$D_A = 4\bar{R}(1+c)^2/3. \tag{5b}$$

These expressions connect the apparent domain sizes D_A and D_V with the real dimensions (radius or diameter) of the crystallites. For a monodisperse system of spheres of diameter D, $c = 0$ and the following holds:

$$D = (4/3)D_V = (3/2)D_A. \tag{6}$$

3.2. Warren–Averbach analysis

In the absence of other microstructural information, which would be a basis for a physically sound broadening model, it is preferred that a model-unbiased approach be used. The Warren–Averbach (1952) (W-A) approach is frequently used for this purpose. It has to be applied carefully to avoid potentially serious systematic errors (see, for instance, Young *et al.*, 1967; Delhez *et al.*, 1980). The method requires the

Table 3
Results of the Warren–Averbach analysis.

Area-weighted D_A and volume-weighted D_V domain sizes, and root-mean-square strain (RMSS) at $D_V/2$. The standard uncertainties are estimated as about 5%.

				RMSS = 0	
	D_A (Å)	D_V (Å)	RMSS (10^{-4})	D_A (Å)	D_V (Å)
Birmingham	177	238	4.4	159	228
Le Mans	198	241	6.6	181	226
ESRF	195	213	0†	187	224
NSLS	196	234	4.1	189	229
ILL	188	228	4.5	176	224
NIST	194	251	7.1	167	230
ISIS	165	248	5.0	177	240

† Set to zero; MSS is a small negative number.

Fourier transform of a physically broadened profile; we used profiles obtained by Bayesian deconvolution. In this way, a direct comparison of results obtained by the W-A analysis and the model of lognormal size distribution of spherical crystallites is possible.

The physically broadened profiles obtained by Bayesian deconvolution in real space were Fourier transformed. We used the Warren–Averbach (1952) approximation to separate the effects of size and strain broadening and carried out the line-broadening analysis in a customary way [see Warren (1969) for a full description of the method] to obtain root-mean-square strain (RMSS) averaged over a distance in real space, perpendicular to diffracting planes, and an apparent area-weighted domain size D_A (Bertaut, 1949). For a comparison with the volume-weighted domain size that follows from Rietveld refinement, we also evaluated the apparent volume-weighted domain size as a sum:

$$D_V = a_3 \sum_{L=-\infty}^{\infty} A_S(L); \quad a_3 = \lambda/4|\sin\theta_{end} - \sin\theta_{cen}|, \quad (7)$$

where the length a_3 depends on the span of the profiles (θ_{cen} and θ_{end} denote the positions of the profile centroid and the point where the intensity reaches a background level). In practice, the sum is evaluated up to a Fourier number after which Fourier coefficients begin to oscillate after reaching near zero; for our data this value was about 400 ± 50 Å.

The Warren–Averbach (1952) separation method indicated very small if nonexistent anisotropy. Therefore, we applied the line-broadening analysis to all diffraction lines, thus averaging the results over the same reflections as in the LNSDSC method. After the separation, the size coefficients are plotted as a function of averaging distance L. A small 'hook' effect in $A_S(L)|_{L\to 0}$ (Warren, 1969) was regularly observed for all the data. This effect is normally attributed to an incorrectly (too high) estimated background (Delhez *et al.*, 1980) or to small-angle tilt boundaries, as proposed by Wilkens (1979). The former is difficult to avoid because the tails of the size-broadened profile fall off with the inverse square distance from the peak, as already shown by Wilson (1962, 1963). Thus, all the profiles in a diffraction pattern overlap even for samples with cubic symmetry, and the true background is difficult to reach without making an assumption on the functional form of peak profiles. The latter is highly unlikely in our sample because the presence of dislocations would introduce line-broadening anisotropy, whereas our results show line broadening to be isotropic. The 'hook' effect increases the value of D_A if the derivative is taken at $L = 0$. We corrected for this effect by fitting the linear part of the curve, in the region 40–90 Å, and determined the root of the parallel straight line passing through unity on the y axis. Both the area-weighted and the volume-weighted apparent domain sizes are reported in Table 3. The values of root-mean-square strain (RMSS) at $D_V/2$ are also given in Table 3. Although the RMSS varies significantly among different data sets, its magnitude is relatively small, compared with the size effect. It can be argued that such a small strain can be neglected; in this way, a potentially significant systematic error because of the Warren–Averbach (1952) size–strain separation is avoided. We also quote domain sizes with zero strain in Table 3. Volume-weighted domain size was calculated analogously to equation (7), but with the average sum of the real Fourier coefficients instead of size coefficients. Area-weighted domain size was determined from the slope to the real Fourier coefficients, averaged over all reflections, in the same way as for the D_A. It is evident that even such a relatively small strain has a large influence on both, but especially on the area-weighted domain size.

3.3. Rietveld refinement

Rietveld refinement is becoming progressively more popular for nonstructural applications, such as texture (Von Dreele, 1997; Matthies *et al.*, 1997) and residual-stress (Ferrari & Lutterotti, 1994; Daymond *et al.*, 1997; Balzar *et al.*, 1998; Popa & Balzar, 2001) determination. It is common practice to estimate domain size and strain values from the refined profile width parameters. A comprehensive study on line-broadening analysis and Rietveld refinement has been presented by Delhez *et al.* (1993). Even for purely structural use, it is necessary to account for integrated peak intensity in a correct way to obtain reliable structural information. An accurate modeling of line width is a necessary prerequisite for all these cases. However, there is a need to clarify the procedures to estimate domain size and strain from refined profile width parameters. The original Rietveld program (Rietveld, 1969) was designed for low-resolution neutron diffraction measurements that yield a simple Gaussian line shape. Consequently, line-width models had to be improved to accommodate high-resolution neutron instruments and especially X-ray laboratory and synchrotron data with intrinsically more complex line shapes. We used the Rietveld refinement program contained in the *GSAS* suite (Larson & Von Dreele, 2001) for all the refinements. However, the discussion here applies to other programs as well because the profile shapes used in major Rietveld programs are relatively uniform.

The line profile model for the CW data, which is introduced in all major Rietveld-refinement programs, is a generalization of the Thompson *et al.* (1987) approach. It implicitly assumes that the observed and constituent line profiles are Voigt functions (Balzar & Ledbetter, 1995). Because a convolution

of any number of Voigt functions is also a Voigt function, one can write the following expressions for Gaussian and Lorentzian observed line widths (CW data):

$$\Gamma_G^2 = U\tan^2\theta + V\tan\theta + W + P/\cos^2\theta \qquad (8a)$$

and

$$\Gamma_L = X/\cos\theta + Y\tan\theta + Z. \qquad (8b)$$

Here, Γ is the full width at half-maximum (FWHM) of the line profile, U, V, W, X, Y and Z are refinable parameters and L and G denote Lorentzian and Gaussian profiles, respectively. Equation (8*a*) is based on the Caglioti *et al.* (1958) paper, which modeled neutron diffraction line shapes in terms of collimator and monochromator transmission functions in the Gaussian approximation. The last term in (8*a*) was added by Young & Desai (1989) and describes the Gaussian contribution to the Scherrer (1918) size broadening:

$$\beta_S = \lambda/D_V\cos\theta, \qquad (9)$$

where λ is the wavelength and D_V is volume-weighted domain size. Here, we do not need to correct for the shape of crystallites by using the Scherrer constant K because D_V is the volume-weighted thickness perpendicular to the diffracting planes (Wilson, 1962). Equation (8*b*) is the Lorentzian line width and includes contributions from Lorentzian size broadening X and Lorentzian strain broadening Y; Z is customarily set to zero in most Rietveld refinement programs. The term that varies with $\tan\theta$ stems from the Stokes & Wilson (1944) definition of the maximum (upper limit) of strain:

$$e = \beta_D/4\tan\theta. \qquad (10)$$

Hence, it is easy to recognize from equations (8) that parameters X and P will relate to size broadening and Y and U to strain broadening. However, some instrumental contributions have similar dependence on diffracting angle and that contribution has to be carefully separated to obtain accurate information about domain size and strain from line broadening.

The following expressions are equivalent to equations (8) for the TOF data (Larson & Von Dreele, 2001):

$$\Gamma_G^2 = \sigma_1^2 d^2 + \sigma_2^2 d^4 + \sigma_0^2 \qquad (11a)$$

and

$$\Gamma_L = \gamma_1 d + \gamma_2 d^2 + \gamma_0. \qquad (11b)$$

Here, σ_1^2 and γ_1 model Gaussian and Lorentzian strain broadening and σ_2^2 and γ_2 model Gaussian and Lorentzian size broadening. Then, instead of equations (9) and (10), we use

$$D_V = \mathrm{DIFC}/\beta_S; \quad e = \beta_D/2\mathrm{DIFC}, \qquad (12)$$

where DIFC is the diffractometer constant connecting d spacing and the neutron time of flight TOF:

$$\mathrm{TOF} = \mathrm{DIFC}\,d + \mathrm{DIFA}\,d^2 + \mathrm{ZERO}. \qquad (13)$$

The second-order term DIFA is small and can be neglected here.

This model is certainly very simplified and not flexible enough to describe all possible size- and strain-related effects on diffraction line shapes. Currently, there is ample interest to include modeling of line widths in Rietveld refinement based on physical models; however, it is difficult to include models for all possible physical origins of broadening and even more importantly, to preclude improper use of such a Rietveld program by an inexperienced user, as different refinable parameters may have a similar angle dependence and thus strongly correlate during the refinement.

3.3.1. Instrumental broadening. Every instrument introduces some amount of broadening that has to be properly corrected in order to obtain reliable information about the sample under investigation. However, there are significant differences for different types of radiation and instrumental setups. Each instrument is discussed in turn.

Laboratory X-rays. Major contributions are from wavelength dispersion and slits, respectively (Klug & Alexander, 1974):

$$\beta_L = 2(\Delta\lambda/\lambda)\tan\theta; \quad \beta_G = \mathrm{const}. \qquad (14)$$

Therefore, to the first approximation, instrumental broadening can be modeled by refinement of only two parameters, Y and W (Balzar & Ledbetter, 1995).

However, for a careful study, it is necessary to adjust other parameters in equations (8), as needed. We used *GSAS* profile function #2 (Howard, 1982) because peaks were sufficiently symmetric for both laboratory data sets.

Synchrotron. Observed profiles are well described by a Voigt function and its approximations, pseudo-Voigt and Pearson VII. Because of a high flexibility and frequent adjustment of optical elements, the profile shape can vary significantly. In general, all the parameters in equations (8) were refined for a standard sample. We used *GSAS* profile function #3 (Finger *et al.*, 1994), which is superior to function #2 in the case of high asymmetry, to account properly for asymmetry at lower angles due to axial divergence of the beam. The axial divergence effects are here potentially very important because of a tendency to use shorter wavelengths, especially at third-generation synchrotrons.

Neutron CW. All three Gaussian terms U, V and W in equation (8*a*) have to be refined. Additionally, high-resolution instruments may need refinement of Lorentzian parameters, due to the greater significance of the monochromator contribution (that is, intrinsic width with long tails), which is here approximated by a Lorentzian function. We also used *GSAS* profile function #3 (Finger *et al.*, 1994), as the axial divergence asymmetry is introduced in particular by large samples and tall detectors.

Neutron time-of-flight (TOF). A thorough description of a complex profile shape given by TOF neutron measurements is given in the *GSAS* manual (Larson & Von Dreele, 2001). We used *GSAS* profile function #3 (convolution of back-to-back exponentials with a pseudo-Voigt function) for high-resolution instruments, and refined α_1, β_0, β_1, σ_0 and γ_0 for a standard sample.

Instrument resolution can potentially play an important role in line-broadening analysis, which was the main reason to collect the data with different radiation and instrument geometries. Fig. 2 plots the instrument resolution, $\Delta d/d$, calculated from the FWHM of the instrumental standard profile (sample S2), as obtained by Rietveld refinement of line profile parameters. Both synchrotron and ISIS resolution decreases little with the increase in d spacing. There are some surprising findings. All the instruments have comparable resolution at smaller d values (~0.7–0.9 Å), whereas at 3.5 Å, resolution differs by an order of magnitude. At smaller d values, ESRF shows the best resolution, but it is second to the NSLS at larger d values! One has to keep in mind, however, that the sample S2 likely has a small amount of residual physical broadening. This will skew the results shown more for instruments with smaller intrinsic line broadening, namely the synchrotron and ISIS data.

3.3.2. Physical broadening. To obtain a physical contribution to the broadening, it is sufficient to refine four parameters in equations (8) or (11). Before estimating physical broadening of a sample under investigation (sam), these refined values have to be corrected for instrumental effects, which were determined by refinement of line profiles of the sample S2 (stand). We can write

$$\Gamma_{\rm eff} = \Gamma_{\rm sam} - \Gamma_{\rm stand}, \qquad (15)$$

where Γ stands for X, P, U and Y for the CW data, and σ_1^2, σ_2^2, γ_1, and γ_2 for the TOF data. The effective value (eff) depicts the pure physically broadened profile parameters.

As the parameters in equations (8) and (11) are the FWHM, they should be converted to integral breadths of size-broadened and strain-broadened profiles before calculating associated domain size and strain values. Conversion factors are (Langford, 1978)

$$\beta_{\rm L}/\Gamma_{\rm L} = \pi/2 \quad \text{and} \quad \beta_{\rm G}/\Gamma_{\rm G} = (1/2)(\pi/\ln 2)^{1/2}, \qquad (16)$$

where $\Gamma_{\rm L}$ and $\Gamma_{\rm G}$ are calculated from the effective parameters determined using equation (15). However, *GSAS* internally reduces the Gaussian FWHM by the factor $(8\ln 2)^{1/2}$ (Larson & Von Dreele, 2001); thus the second equation in the case of *GSAS* should be taken as

$$\beta_{\rm G}/\Gamma_{\rm G} = (2\pi)^{1/2}. \qquad (17)$$

Then, the Lorentzian and Gaussian integral breadths are combined for both the size and the strain parts according to the relation (Langford, 1978)

$$\beta_i = (\beta_{\rm G})_i \exp(-k^2)/[1 - {\rm erf}(k)]; \quad k = \beta_{\rm L}/\pi^{1/2}\beta_{\rm G}, \qquad (18)$$

where i stands for S or D. Only now can $\beta_{\rm S}$ and $\beta_{\rm D}$ be related to the corresponding values of $D_{\rm V}$ and e, according to equations (9) and (10) or (12).

The conversion equations (16) are equivalent to the alternative numerical expressions connecting the integral breadth β and FWHM Γ of a pseudo-Voigt profile, as customarily used in Rietveld refinement programs (Thompson *et al.*, 1987).

We give the results for both $D_{\rm V}$ and e in Table 4, where we designate the volume-weighted domain size, as obtained from Rietveld refinement, as $D_{\rm R}$.

3.3.3. Refinement procedure. In the ceria crystal structure, all atoms are in special positions ($Fm\bar{3}m$, $a \simeq 5.41$ Å). Therefore, the only structural parameters refined were the lattice parameter and the temperature factors. The global parameters included the scale factor, the 2θ zero correction, and background parameters (four terms of the $Q^{2n}/n!$ series for the ISIS measurements and three terms of the cosine Fourier series for all other measurements except ESRF, where five coefficients had to be refined) for all the data sets. For the flat-plate geometries (both laboratory X-rays and NSLS measurements), sample transparency and shift corrections were refined. Additionally, the refinement of the surface-roughness correction (Suortti, 1972) lessened or completely corrected a problem of negative temperature factors for this geometry. A Debye–Scherrer absorption correction (function #0 in *GSAS*) was refined only for ISIS and ESRF measurements, as it is significant only for energy-dependent (TOF) data or the X-ray Debye–Scherrer geometry. A preferred-orientation-correction refinement was attempted, but did not yield significant improvement for any of the patterns.

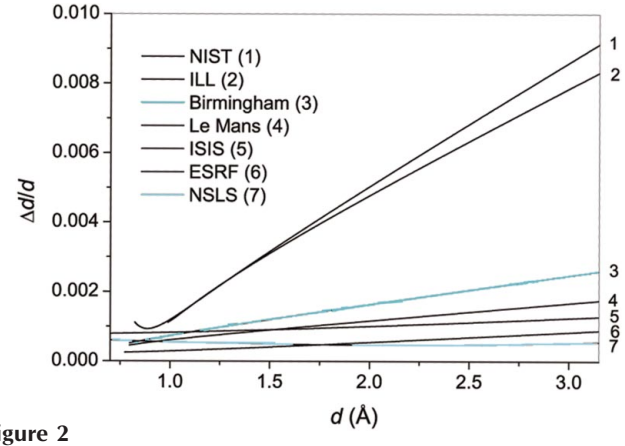

Figure 2
Resolution function $\Delta d/d$ as a function of interplanar spacing d for all instruments, as calculated from the FWHM obtained by Rietveld refinement, for the sample S2.

Table 4
Results of the Rietveld refinement.

Volume-weighted domain size $D_{\rm R}$ and strain e. The ratio of the Gaussian $\beta_{\rm G}$ to Lorentzian $\beta_{\rm L}$ integral breadth of the size profile is also shown.

	Comments	$D_{\rm R}$ (Å)	$\beta_{\rm G}/\beta_{\rm L}$	e (10^{-4})	$D_{\rm R}$ (Å) for $e = 0$†
Birmingham	Both strain terms → 0	227 (3)	0.85 (2)	0	227 (3)
Le Mans	Gauss strain term → 0	235 (2)	1.01 (1)	2.2 (1)	224 (1)
ESRF		223 (1)	0.704 (7)	1.5 (1)	219 (1)
NSLS	Gauss strain term → 0	236 (2)	0.84 (1)	2.3 (1)	224 (1)
ILL	Gauss strain term → 0	221 (3)	0.83 (2)	0.1 (3)	220 (2)
NIST	Lorentz strain term → 0	231 (6)	0.74 (4)	4.5 (8)	216 (4)
ISIS	Lorentz strain term → 0	232 (1)	0.831 (8)	5.5 (2)	224 (1)

† Strain-related parameters set to the values of the instrumental standard sample during the refinement.

We initially refined diffraction patterns of the standard sample. Profile parameters were refined according to the procedure described in the preceding paragraph. For the broadened pattern, all the parameters were then fixed to these values, except for X, P, U and Y for the CW data and σ_1^2, σ_2^2, γ_1, and γ_2 for the TOF data. For all data sets, except ESRF, either the Gaussian or Lorentzian effective (corrected for the instrumental broadening) strain term refined to zero. If a strain-related parameter for the sample S1 refined to a smaller value than for the standard sample (S2), the parameter was fixed to the value obtained for the standard sample in the subsequent cycles. The final refined diffraction patterns for all instruments are available *via* the IUCr electronic archives.[4]

For all the data sets, both Lorentzian and Gaussian size parameters refined to a non-zero value. Strain-related parameters were evidently less significant, although they varied in magnitude among different instruments (see Table 4). To compare the results with the values obtained by the LNSDSC method, we also give the value of volume-weighted domain size with the strain-related parameters set to the values determined for the standard sample, that is, the broadening due to the size effect only.

4. Discussion of line-broadening results

The intrinsic (instrumental) line width is potentially an important parameter in line-broadening analysis. It is advantageous that the physical broadening, which contains sought information, be more pronounced than the instrumental broadening, which requires the undesirable correction of observed profiles for the instrumental effect. Therefore, analogously to the signal-to-noise ratio, one can presume that a larger dimensionless ratio of integral breadths of the physical and instrumental profiles β_p/β_g should increase the precision of line-broadening analysis. For this reason in particular, we tried to include measurements at different resolutions. In Fig. 3, we show the 220 diffraction lines for both samples S1 and S2. It is evident that the ratio β_p/β_g changes by an order of magnitude among the instruments. However, the results indicate that the resolution does not appear to be a decisive factor in obtaining accurate values for the domain size and strain. Of course, as physical broadening becomes smaller, an instrument with a narrow intrinsic broadening is expected to be more advantageous for line-broadening studies.

The comparison of results in Tables 2–4 indicates that the uncertainty due to different analysis methods is much more significant than the influence of a particular instrument. The small scatter of results among different instruments is especially evident for a model with an assumed lognormal size distribution of spherical crystallites, which is most likely due to a relatively simple physical model with few refined parameters. As a comparison, in a Rietveld refinement there is a possibility that other parameters with similar angle dependence compensate for the size or strain parameter during the refinement; in particular, specimen transparency or absorption, depending on the geometry and radiation, introduce line broadening and would therefore be expected to influence line-broadening parameters. In the refinements conducted, the correlation matrix did not indicate a strong correlation of the size and strain-related profile parameters with other parameters. The second potential cause of discrepancy is the background level, as different models were used for Bayesian deconvolution and Rietveld refinement. A 'hook' effect that was observed in the W-A analysis, might indicate that the background was determined as too high; this would produce the effect of underestimating broadening in the W-A analysis. It is not clear how much the background level affects the profile parameters in Rietveld analysis. This is unlikely to be a significant problem in this case because of relatively few Bragg peaks in the pattern.

The most important element influencing uncertainty of the results appears to be the strain; the scatter in domain sizes between different instruments is significantly diminished by setting strain to zero in Tables 3 and 4. The value of strain seems to depend greatly on the method of analysis used. For instance, from Tables 3 and 4. we see that on the same set of data one method can yield zero strain while another yields a large value. The uncertainty is expected to become larger at small strain; however, these differences do not appear to be systematic. Louër *et al.* (2002) recently demonstrated by Rietveld refinement on simulated data (noise was introduced according to a Poisson distribution) for a strain-free sample that a fictitious strain can be obtained if both size and strain-related parameters are allowed to vary. We must also note here that the definitions of strain in the Rietveld and W-A methods are different. An approach to make the two definitions compatible was discussed previously (Balzar & Ledbetter, 1995).

If an average spherical shape and lognormal distribution of crystallites are accepted as plausible, the average crystallite diameter is estimated as 191 (5) Å from all the methods when the strain effect is neglected. Although the crystallite size distribution for the S1 sample is moderately wide [see Popa & Balzar (2002) for discussion and a more detailed characterization], it greatly influences the average diameter (the first distribution moment). As a comparison, in a monodisperse system of spheres with the same apparent volume-weighted domain size, the sphere diameter would be 305 (5) Å, which is an increase of 60%.

It is important to emphasize that, although the ceria sample shows predominately size broadening, the physically broadened profile is not a Lorentzian, as it is very often assumed, but has a significant Gaussian component. Table 4 gives the ratio of the Gaussian to the Lorentzian integral breadth of the size profile, which is in the range 0.704–1.01. Therefore, a Voigt or pseudo-Voigt function is a preferred approximation for a size-broadened profile. It was recently reported (Popa & Balzar, 2002) that broad size distributions (another ceria sample) can produce the so-called 'super-Lorentzian' line profiles; that is, tails fall off more slowly than for a Lorentzian

[4] Supplementary data are available from the IUCr electronic archives (Reference: KS0213). Services for accessing these data are described at the back of the journal.

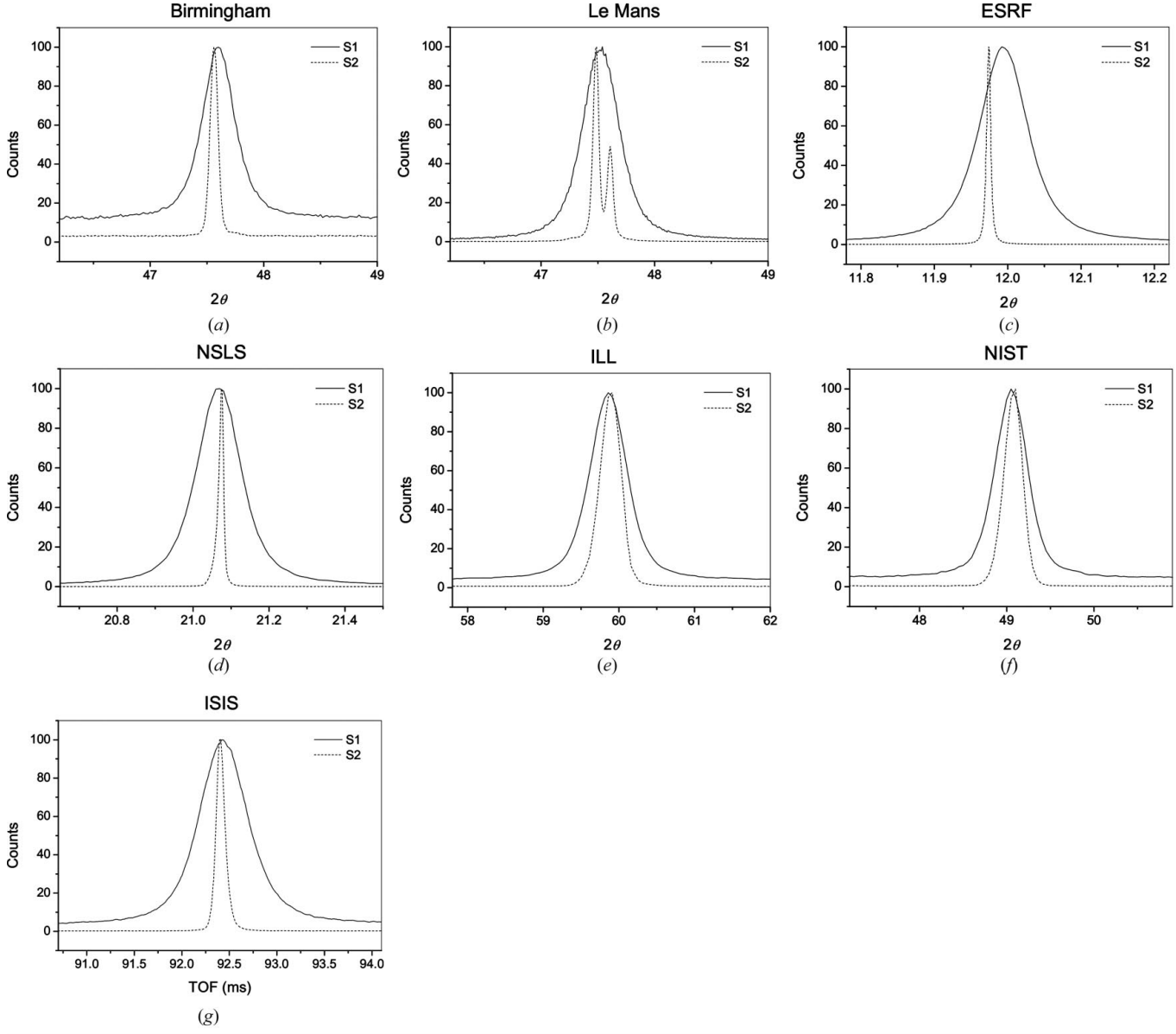

Figure 3
220 diffraction lines of S1 and S2 samples, normalized to the same maximum peak height, for all the instruments.

function. Such a line profile can be successfully modeled by a lognormal size distribution of spherical crystallites; however, the profiles cannot be modeled by a Voigt function or its approximations and Rietveld refinement using the profile functions discussed here fails.

5. Round robin

5.1. Round-robin preparation and returned results

Here we discuss the round robin. The measurements of the two ceria samples obtained at seven instruments were converted into three formats by using program *POWDER2* (Dragoe, 2001): two-column angle-intensity pairs, *GSAS* (Larson & Von Dreele, 2001) raw data file, and *DBWS-Full-Prof* (Rodriguez-Carvajal, 1990) raw data file. Data and recommendations for analysis were made available to the round-robin participants for download. 18 reports with results were received.[5] An initial screening of results was undertaken to eliminate those with clearly erroneous values of both domain size and strain. After the assessment, the results from 16 participants were included in the final analysis, which could be categorized according to the approach used as follows.

(i) Rietveld (1969) refinement: six reports.

(ii) Warren–Averbach (1952) method: three reports.

(iii) Integral-breadth methods: four reports. Participants used different methods: (*a*) both size-broadened and strain-broadened profiles approximated by a Lorentzian function

[5] The list of all the received results and used techniques have been deposited with the IUCr (Reference: KS0213). Services for accessing these data are described at the back of the journal.

(Lorentz–Lorentz, LL) (Klug & Alexander, 1974); (*b*) size-broadened profile approximated by the Lorentzian function and strain-broadened profile by the Gaussian function (Lorentz–Gauss, LG) (Klug & Alexander, 1974); (*c*) both size-broadened and strain-broadened profiles approximated by a Voigt function following the Langford (1980) approach (VV1) and the Balzar (1992) approach (VV2).

(iv) 'Fundamental parameter' approach (Cheary & Coelho, 1992): three reports.

(v) Single-line approach (Hall & Somashekar, 1991): one report.

(vi) Special: two reports. Although these methods were previously described in the literature, these particular results were obtained by using unpublished methods. They could be characterized as: monodisperse system of spherical crystallites and lognormal distribution of spherical crystallites.

The participants used from one to three different approaches on a different number of data sets. All considered round-robin results yielded positive domain size. Most of the results gave very small positive or negative, or zero values of strain. The absence of substantial strain was expected for this material and is in accord with already published results (Audebrand *et al.*, 2000). However, some participants reported strains significantly larger than zero; maximum strain reported was 0.04 (4%), with the average value of 0.004 (9), considering only the results that reported values of strain larger than zero. These results were not routinely disqualified unless domain sizes were clearly incorrect.

Instrumental broadening was taken into account in different ways, depending on the chosen analytical route. In all cases, except the 'fundamental parameter' (FP) approach (Cheary & Coelho, 1992), instrumental broadening was corrected for by using the provided measurements of annealed ceria sample S2. The FP approach was applied only to the Le Mans measurements and instrumental parameters were estimated for the particular diffractometer from the provided details.

5.2. Discussion of round-robin results

To be able to compare the results, an attempt was made to scale all the reported parameters into groups of results that are identically defined. As is customary in this field, we considered two groups of size–strain quantities: apparent volume-weighted domain size (D_V) and the upper limit of strain (e), which result from integral-breadth and similar methods of line-broadening analysis (Klug & Alexander, 1974), and apparent area-weighted domain size (D_A) and root-mean-square strain (RMSS), which follow from Fourier and related techniques (Warren, 1969). Both measures of domain size represent weighted averages of the average dimension along the diffraction vector and can be related to the true crystallite size if both shape and size distribution are known. Because not all the data sets were analyzed by the participants, the averages and standard uncertainties reported here were calculated from a minimum of three to a maximum of 43 results reported by the participants.

The values for D_V and D_A are reported in Figs. 4 and 5. Despite standard uncertainties being relatively large for the former, all the methods gave results that agree reasonably well. This is expected for samples without substantial strain broadening, whereas there are systematic differences given by different methods for samples with comparable size-broadening and strain-broadening effects (see, for instance, Balzar & Popović, 1996). However, an indication that the results should be more carefully assessed is given in Fig. 6, where the average domain sizes, both volume- and area-weighted, are plotted for different instruments. The first impression is that D_A values show much less scatter and with a significantly smaller standard uncertainty, similar to results in Fig. 5. An inspection of the D_V values shows that the results are clustered in two regions: below 250 Å with the mean (226 ± 9) Å

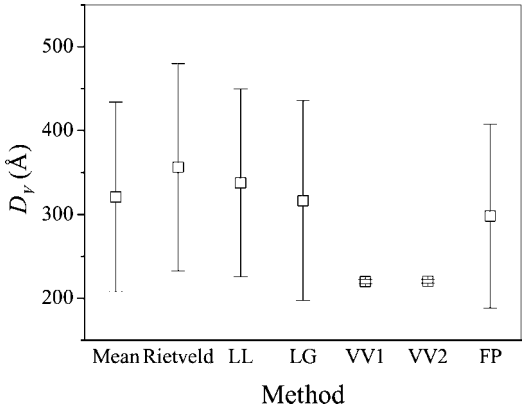

Figure 4
Average apparent volume-weighted domain size for different methods. The mean is an average over all the results, LL is the Lorentz–Lorentz integral-breadth method (Klug & Alexander, 1974), LG is the Lorentz (size)–Gauss (strain) integral-breadth method (Klug & Alexander, 1974), VV1 is the double-Voigt method following Langford (1980), VV2 is the double-Voigt method following Balzar (1992), and FP is the 'fundamental parameter' approach (Cheary & Coelho, 1992).

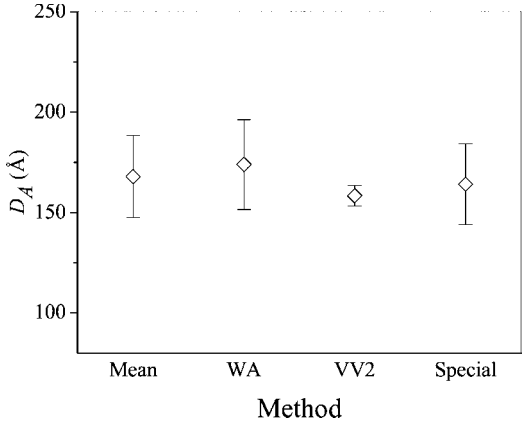

Figure 5
Average apparent area-weighted domain size for different methods. The mean is an average over all the results, WA is the Warren–Averbach (1952) method, VV2 is the double-Voigt method following Balzar (1992), and 'Special' includes various results obtained by the Fourier Rietveld method (Le Bail, 1999) and the single-line Fourier method (Hall & Somashekar, 1991).

and above 250 Å with a much larger scatter, (390 ± 100) Å. Participants that obtained results in the latter group did not analyze either NSLS or ESRF synchrotron data, which explains their smaller standard uncertainty in Fig. 6 (the means are significantly different only at better than 1% significance level).

The reason why results for D_V are clustered in two separate groups can be understood in terms of the strain, as some participants reported strain significantly larger than zero. Therefore, part of the line broadening was attributed to the strain effects, which gave larger domain size and systematically shifted the averages in Fig. 4 toward the larger domain sizes. Participants using the double-Voigt approaches (VV1 and VV2 in Fig. 4) did not detect strain, which explains the lower values for domain size. Another possible reason for discrepancy is an oversimplified analytical model for the size-broadened profile; that is, a single Lorentzian function. This is inherent to Lorentz–Lorentz (LL) and Lorentz–Gauss (LG) integral-breadth methods (Klug & Alexander, 1974). However, for strain-free samples, if the observed profile is fitted with a Voigt (or related) function and the subsequent analysis is performed according to one of the simplified integral-breadth methods, the difference between simplified and double-Voigt methods is minimal.

In Rietveld refinement, the situation is different because it is up to a user to refine particular parameters. For instance, most of the participants that obtained a measurable strain effect did not refine the Gaussian size term, proportional to $1/\cos^2\theta$ [see equation (8*a*)]. Because there was a significant Gaussian component to physically broadened line profiles, it was probably erroneously absorbed into the Gaussian strain term (proportional to $\tan^2\theta$). This fact suggests caution when performing Rietveld refinements; although strain and size Gaussian terms have different angle dependences, the difference could be compensated by refinement of some other parameters that strongly correlate with profile parameters, in particular if the diffraction pattern was collected over a limited angular range. A recommended procedure to extract size and strain values by Rietveld refinement is extensively discussed in §3.3. Another factor that should be considered when refining size- and strain-related parameters is noise in the data, which could result in the fictitious strain, as described by Louër *et al.* (2002).

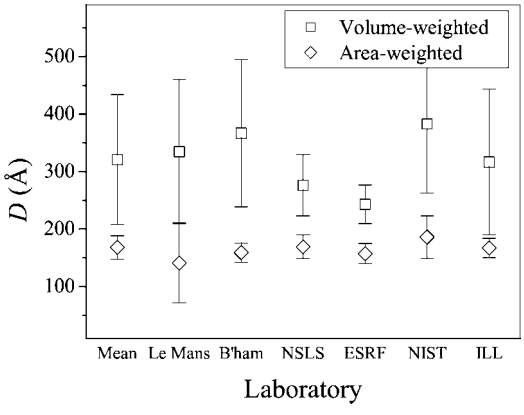

Figure 6
Average apparent volume-weighted and area-weighted domain size for different instruments. The mean is an average over all the results.

Participants that used Fourier methods that yield the D_A reported no significant strain values, which explains the uniformity of the D_A results. However, because some Fourier methods used a simple Lorentzian model for a size-broadened profile, it is interesting to note that these results did not give overestimated values of domain size. This is possible to understand in the framework of Voigt-function modeling in the Fourier approach; the D_A depends only on a Lorentzian part of the size-broadened profile (Balzar & Ledbetter, 1993).

6. Summary and conclusions

In summary, we have described the preparation of a ceria round-robin sample and line-broadening results obtained by three methods on seven sets of measurements collected with both laboratory and synchrotron X-rays, and from constant-wavelength and time-of-flight neutron sources. Furthermore, we have given an account of the results of the size–strain round robin on line-broadening analysis methods (sponsored by the Commission on Powder Diffraction of the International Union of Crystallography). The ceria round-robin sample has a relatively small strain; if strain is constrained to zero, all three methods agree well. The main problem in the line-broadening analysis seems to be the size–strain separation, for which different methods yield significantly different results. The scatter of strain values appears more significant in the Rietveld analysis, which may indicate possible correlation with other refinable parameters. All three methods have obvious limitations and advantages. While a model based on an accurate physical description of the sample is always preferred and in this case has shown good results, it has to apply to at least a majority of grains in a polycrystalline aggregate. Warren–Averbach (1952) analysis is the least-biased phenomenological approach, but cannot be applied in cases of significant peak overlap or large strains that do not follow a Gaussian distribution, which is difficult to know *a priori*. Therefore, Rietveld refinement or a similar full-powder-pattern method may be the only alternative approach for an arbitrary sample. However, most Rietveld programs model line profiles in terms of the simple multiple Voigt functions, which worked well for the present sample, but should be generalized to include non-Voigtian line profiles, such as 'super-Lorentzians' or possible other shapes.

The size–strain round robin was organized to assess the accuracy of the determination of size and strain values, as derived by different methods, using measurements collected at seven different instruments. The results of diffraction line-broadening analysis were received from 18 participants and 16 were included in this report. The average apparent domain sizes, calculated from all the reported values, are as follows:

$$D_V = (320 \pm 110)\ \text{Å}; \quad D_A = (168 \pm 21)\ \text{Å}. \qquad (19)$$

An inspection of the Rietveld refinement results has shown that a significant number of participants did not refine the

Gaussian domain-size term, which has likely attributed some of the size-related broadening to other effects. This has, in effect, increased the average volume-weighted domain size in equation (19). If only the results obtained without significant strain broadening are considered, the average values are as follows:

$$D_V = (226 \pm 9)\ \text{Å}; \quad D_A = (168 \pm 21)\ \text{Å}. \qquad (20)$$

In the first part of this paper, domain sizes were calculated using three approaches: an assumed lognormal size distribution of spherical crystallites (Popa & Balzar, 2002), the Warren–Averbach (1952) method, and Rietveld (1969) refinement. An average of all the results (where the values of the domain sizes obtained with strain different from zero for the last two approaches are considered) gives the following values:

$$D_V = (231 \pm 5)\ \text{Å}; \quad D_A = (179 \pm 5)\ \text{Å} \qquad (20)$$

Thus, both the volume-weighted and area-weighted apparent domain sizes agree within a single standard uncertainty.

Additionally, based on the analysis of the round-robin results, several observations can be made, as follows.

(i) All the methods used for line-broadening analysis gave results that fall within a single (largest) standard uncertainty. This is not likely to be expected in general, but is probably a consequence of the absence of strain in the round-robin sample.

(ii) When using Rietveld refinement to obtain size and strain values, both Lorentzian and Gaussian contributions to the size-broadening term should be refined. If only the Lorentzian term is refined, Gaussian size broadening can be misrepresented as strain broadening or some other correlating effect, which systematically alters the results for domain size. For instance, the results show that this change can be quite large: from 226 Å to 390 Å, which is an increase of 73%!

(iii) The area-weighted domain size, as obtained from Fourier methods, is less sensitive to this effect because the resulting domain size does not depend on the Gaussian part in the Voigtian approximation for the size-broadened profile.

All the round-robin participants are gratefully acknowledged for their time and effort. We are also indebted to the Commission on Powder Diffraction (CPD) of the International Union of Crystallography (IUCr) for supporting the size–strain round robin. Lachlan Cranswick is acknowledged for initiating the idea that led to the size–strain round robin. The help of Nita Dragoe with data conversion is appreciated. We thank Richard Ibberson and the Central Laboratory of the Research Councils ISIS Facility for time on HRPD.

References

Armstrong, N., Kalceff, W., Cline, J. P. & Bonevich, J. (2004). *Diffraction Analysis of the Microstructure of Materials*, edited by E. J. Mittemeijer & P. Scardi, pp. 187–227. Berlin: Springer.
Audebrand, N., Auffrédic, J.-P. & Louër, D. (2000). *Chem. Mater.* **12**, 1791–1799.
Balzar, D. (1992). *J. Appl. Cryst.* **25**, 559–570.
Balzar, D. (1999). *Defect and Microstructure Analysis by Diffraction*, edited by R. Snyder, J. Fiala & H. J. Bunge, pp. 94–126. IUCr/Oxford University Press.
Balzar, D. & Ledbetter, H. (1993). *J. Appl. Cryst.* **26**, 97–103.
Balzar, D. & Ledbetter, H. (1995). *Adv. X-ray Analysis*, **38**, 397–404.
Balzar, D. & Popović, S. (1996). *J. Appl. Cryst.* **29**, 16–23.
Balzar, D., Von Dreele, R. B., Bennett, K. & Ledbetter, H. (1998). *J. Appl. Phys.* **84**, 4822–4833.
Berkum, J. G. M. van (1994). PhD thesis, p. 136, Delft University of Technology.
Bertaut, E. F. (1949). *C. R. Acad. Sci. Paris*, **228**, 187–189, 492–494.
Caglioti, G., Paoletti, A. & Ricci, F. P. (1958). *Nucl. Instrum. Methods*, **3**, 223–228.
Čerňanský, M. (1999). *Defect and Microstructure Analysis by Diffraction*, edited by R. Snyder, J. Fiala & H. J. Bunge, pp. 613–651. IUCr/Oxford University Press.
Cheary, R. W. & Coelho, A. (1992). *J. Appl. Cryst.* **25**, 109–121.
Daymond, M. R., Bourke, M. A. M., Von Dreele, R. B., Clausen, B. & Lorentzen, T. (1997). *J. Appl. Phys.* **82**, 1554–1562.
Delhez, R., de Keijser, Th. H. & Mittemeijer, E. J. (1980). *Accuracy in Powder Diffraction*, *Natl Bur. Stand. Spec. Publ. No. 567*, pp. 213–253.
Delhez, R., de Keijser, Th. H., Langford, J. I., Louër, D., Mittemeijer, E. J. & Sonneveld, E. J. (1993). *The Rietveld Method*, edited by R. A. Young, pp. 132–166. IUCr/Oxford University Press.
Dragoe, N. (2001). *J. Appl. Cryst.* **34**, 535.
Ferrari, M. & Lutterotti, L. (1994). *J. Appl. Phys.* **76**, 7246–7255.
Finger, L. W., Cox, D. E. & Jephcoat, A. P. (1994). *J. Appl. Cryst.* **27**, 892–900.
Hall, I. H. & Somashekar, R. (1991). *J. Appl. Cryst.* **24**, 1051–1059.
Howard, C. J. (1982). *J. Appl. Cryst.* **15**, 615–620.
Kennett, T. J., Prestwich, W. V. & Robertson, A. (1978). *Nucl. Instrum. Methods*, **151**, 285–292.
Klug, H. P. & Alexander, L. E. (1974). *X-ray Diffraction Procedures*, 2nd ed. New York: John Wiley.
Krill, C. E. & Birringer, R. (1998). *Philos. Mag. A*, **77**, 621–640.
Krivoglaz, M. A. (1996). *X-ray and Neutron Diffraction in Nonideal Crystals*. Berlin: Springer.
Langford, J. I. (1978). *J. Appl. Cryst.* **11**, 10–14.
Langford, J. I. (1980). *Accuracy in Powder Diffraction*, *Natl Bur. Stand. Spec. Publ. No. 567*, pp. 255–269.
Langford, J. I. (1992). *Accuracy in Powder Diffraction II*, *NIST Spec. Publ. No. 846*, pp. 110–126.
Langford, J. I., Louër, D. & Scardi, P. (2000). *J. Appl. Cryst.* **33**, 964–974.
Larson, A. C. & Von Dreele, R. B. (2001). *General Structure Analysis System GSAS*, Los Alamos National Laboratory Report.
Le Bail, A. (1999). *Defect and Microstructure Analysis by Diffraction*, edited by R. Snyder, J. Fiala & H. J. Bunge, pp. 535–555. IUCr/Oxford University Press.
Louër, D., Auffrédic, J. P., Langford, J. I., Ciosmak, D. & Niepce, J. C. (1983). *J. Appl. Cryst.* **16**, 183–191.
Louër, D., Bataille, T., Roisnel, T. & Rodriguez-Carvajal, J. (2002). *Powder Diffr.* **17**, 262–269.
Louër, D. & Langford, J. I. (1988). *J. Appl. Cryst.* **21**, 430–437.
Matthies, S., Lutterotti, L. & Wenk, H.R. (1997). *J. Appl. Cryst.* **30**, 31–42.
Mittemeijer, E. J. & Scardi, P. (2004). Editors. *Diffraction Analysis of the Microstructure of Materials*. Berlin: Springer.
Popa, N. C. & Balzar, D. (2001). *J. Appl. Cryst.* **34**, 187–195.
Popa, N. C. & Balzar, D. (2002). *J. Appl. Cryst.* **35**, 338–346.
Reefman, D. (1999). *Defect and Microstructure Analysis by Diffraction*, edited by R. Snyder, J. Fiala & H. J. Bunge, pp. 652–670. IUCr/Oxford University Press.
Richardson, W. H. (1972). *J. Opt. Soc. Am.* **62**, 55–59.
Rietveld, H. (1969). *J. Appl. Cryst.* **2**, 65–71.

Rodriguez-Carvajal, J. (1990). *Abstracts of the Satellite Meeting on Powder Diffraction of the XV Congress of the IUCr*, p. 127, Toulouse, France.
Scardi, P. & Leoni, M. (2001). *Acta Cryst.* A**57**, 604–613.
Scherrer, P. (1918). *Gött. Nachr.* **2**, 98–100.
Snyder, R. L., Fiala, J. & Bunge, H. J. (1999). Editors. *Defect and Microstructure Analysis by Diffraction*. IUCr/Oxford: University Press.
Stokes, A. R. (1948). *Proc. Phys. Soc.* (*London*), **61**, 382–391.
Stokes, A. R. & Wilson, A. J. C. (1944). *Proc. Phys. Soc.* (*London*), **56**, 174–181.
Suortti, P. (1972). *J. Appl. Cryst.* **5**, 325–331.
Thompson, P., Cox, D. E. & Hastings, J. B. (1987). *J. Appl. Cryst.* **20**, 79–83.
Ungár, T. (1999). *Defect and Microstructure Analysis by Diffraction*, edited by R. Snyder, J. Fiala & H. J. Bunge, pp. 165–199. IUCr/Oxford: University Press.
Ungár, T., Gubicza, J., Ribárik, G. & Borbély, A. (2001). *J. Appl. Cryst.* **34**, 298–310.
Von Dreele, R. B. (1997). *J. Appl. Cryst.* **30**, 517–525.
Warren, B. E. (1959). *Progress in Metal Physics*, Vol. 8, edited by B. Chalmers, & R. King, pp. 147–202. New York: Pergamon Press.
Warren, B. E. (1969). *X-ray Diffraction*, pp. 251–314. New York: Addison-Wesley.
Warren, B. E. & Averbach, B. L. (1952). *J. Appl. Phys.* **23**, 497.
Wilkens, M. (1979). *J. Appl. Cryst.* **12**, 119.
Wilson, A. J. C. (1962). *X-ray Optics*, 2nd ed., p. 40. London: Methuen.
Wilson, A. J. C. (1963). *Mathematical Theory of X-ray Powder Diffractometry*. Eindhoven: Philips.
Young, R. A. & Desai, P. (1989). *Arch. Nauk Mater.* **10**, 71–90.
Young, R. A., Gerdes, R. J. & Wilson, A. J. C. (1967). *Acta Cryst.* **22**, 155–162.